



XI CONGRESSO NACIONAL DE ENGENHARIA MECÂNICA
DE 07 A 11 DE AGOSTO DE 2022, TERESINA-PI, BRASIL

Nonlinear Dynamics of an Oscillator-Pendulum Energy Harvester

Luã Guedes Costa, guedes@mecanica.coppe.ufrj.br

Virgilio Junior Caetano, vj.caetano@mecanica.coppe.ufrj.br

Marcelo A. Savi, savi@mecanica.ufrj.br

Universidade Federal do Rio de Janeiro, COPPE, Department of Mechanical Engineering, Center for Nonlinear Mechanics - Mecanon, Rio de Janeiro, Brazil

Abstract: Recent developments and concepts in technology as cyber-physical systems, internet of things (IoT), cloud computing and wireless communication procedures require the use of self-powered sensors, actuators and small electronic devices. In this regard, mechanical energy harvesting systems are a promising and viable solution to power standalone devices by converting available environmental mechanical energy into electrical energy, especially through the direct piezoelectric effect. In the latest few decades, several systems have been proposed, many of them containing pendulum-like/bobbing structures in its composition. This work addresses a nonlinear dynamics investigation of a generic oscillator-pendulum energy harvester as a mean to achieve multidirectionality in the energy harvesting process. Numerical simulations are carried out employing the fourth order Runge-Kutta method. A parametric analysis is developed guided by nonlinear dynamics perspective, identifying the nuances and advantages of this kind of system. A performance analysis is carried out focusing on energy harvesting capacity. Results show complex dynamics and increase in energy harvesting capacity for structures with a low ratio between natural frequencies in different directions.

Keywords: Energy Harvesting, Piezoelectric Materials, Nonlinear Dynamics, Chaos, Pendulum Structures.

1. INTRODUCTION

In the last decade, due to the growing establishment of low power standalone devices, the concept of internet of things (IoT), cloud computing and wireless communication procedures, the notion of harvest wasted environmental energy to power these devices and processes has been gaining great traction from several research teams all around the world (Akin-Ponnle and Carvalho, 2021; Tang *et al.*, 2018). In this regard, vibration-based energy harvesting systems are a promising solution that aims to convert wasted mechanical energy of the environment into electrical energy. Piezoelectric materials are one of the most employed transducers to perform the energy conversion through the direct piezoelectric effect (Liu *et al.*, 2018; Sezer and Koç, 2021).

The so called piezoelectric effect is a electromechanical interaction between the mechanical and electrical states within the material. Specifically, the direct piezoelectric effect is a reversible phenomena that relates the mechanical strain and electrical charge (Pierre Curie, 1889). Early developments on vibration-based piezoelectric energy harvesting devices focused on simple linear cantilever beam-type structures due to the high strain in the foundation of its construction (Erturk and Inman, 2011). Experimental and theoretical studies show that this type of conventional cantilever harvester must work near its natural frequency to be efficient, which is incompatible to real applications, as the frequency spectrum of environmental vibrations usually have a wide range of values. To improve the efficiency of cantilever-type energy harvesters, several nonlinear devices were proposed, including the class of multistable devices, that contains magnetoelastic, post-buckled and inverted structures in which bistable (Paula *et al.*, 2015; Costa *et al.*, 2021), tristable (Kumar *et al.*, 2015) and quadstable (Zhou *et al.*, 2017) systems are commonly described to enhance the bandwidth and harvested power. The class of quasi-zero-stiffness cantilever-type systems (Margielewicz *et al.*, 2022) were proposed recently, also showing a great increase in the bandwidth of operation.

Despite the improvements promoted by the addition of different types of mechanical nonlinearities, the analyses of those systems are done considering only one direction in a Cartesian coordinate system, being limited to harvest the energy portion of vibration just in this direction. On the other hand, nature provides vibrations in every direction, for that, authors have proposed the usage of pendulum structures to promote multidirectionality in the energy harvesting process (Wu *et al.*, 2018).

In this work, a reduced order model of a pendulum attached to a conventional cantilever-type piezoelectric energy harvester (a generic oscillator-pendulum) is analyzed. Numerical simulations are carried out employing the fourth order Runge-Kutta method and a parametric analysis is developed guided by a nonlinear dynamics perspective. In this matter, the method proposed by Wolf *et al.* (1985) to determine Lyapunov exponents and Poincaré maps are employed to distin-

guish different types of periodic and aperiodic responses of the system. Also, a performance analysis is done comparing the proposed oscillator-pendulum harvester with its linear version.

2. THEORETICAL MODEL

Consider the theoretical representation of the oscillator-pendulum energy harvester (OPEH) depicted in Figure 1. The general idea of this system is to take advantage of the planar movement of the pendulum to transmit the input energy in the x axis to the z axis. Besides, the set of spring-damper in the x direction serve as a motion amplifier of the movement.

The system is composed by a generic structure of effective mass m_s , and a pendulum-type element of effective mass m_p attached to it by a torsional spring. The stiffness and the damping coefficients of the system are represented by k_i and c_i ($i = x, z, t$), in which the subscripts represents the direction of the property and t refers to the torsional spring. The effects of gravity g are considered and a piezoelectric element is attached in the z direction of the structure, with electromechanical coupling coefficient of θ and a stiffness of k_{pz} . The total capacitance and resistance of the piezoelectric element are represented by R_p and C_p , respectively. Simple resistive circuits of load resistance R_l is connected to the piezoelectric element and the total resistance of the system R is composed by both R_l and R_p . The value of R depends on how the circuit is connected to the piezoelectric element, in series or in parallel. The system is subjected to a harmonic base excitation $\mathbf{r}_b(t) = A \sin(\omega t) [\sin(\mu) \cdot \hat{\mathbf{e}}_x + \cos(\mu) \cdot \hat{\mathbf{e}}_z]$, in which A is the amplitude of the base displacement, ω is the forcing frequency and μ is the angle between directions x and z in which the external excitation is applied. So the absolute structure position can be written as:

$$\begin{aligned} \mathbf{r}_s(t) &= r_{sx}(t) \cdot \hat{\mathbf{e}}_x + r_{sz}(t) \cdot \hat{\mathbf{e}}_z \\ &= [x_b(t) + x_s(t)] \cdot \hat{\mathbf{e}}_x + [z_b(t) + z_s(t)] \cdot \hat{\mathbf{e}}_z \\ &= [x_b(t) + x(t)] \cdot \hat{\mathbf{e}}_x + [z_b(t) + z(t) + z_{st}] \cdot \hat{\mathbf{e}}_z \end{aligned} \quad (1)$$

in which z_{st} is the static deflection of the structure due to gravity action, and can be represented by:

$$z_{st} = \frac{(m_s + m_p) g}{k_z + k_{pz}} \quad (2)$$

The absolute position of the pendulum is of the form:

$$\begin{aligned} \mathbf{r}_p(t) &= r_{px}(t) \cdot \hat{\mathbf{e}}_x + r_{pz}(t) \cdot \hat{\mathbf{e}}_z \\ &= [r_{sx}(t) + x_p(t)] \cdot \hat{\mathbf{e}}_x + [r_{sz}(t) + z_p(t)] \cdot \hat{\mathbf{e}}_z \\ &= [x_b(t) + x(t) + L \sin(\phi(t))] \cdot \hat{\mathbf{e}}_x + [z_b(t) + z(t) + z_{st} + L \cos(\phi(t))] \cdot \hat{\mathbf{e}}_z \end{aligned} \quad (3)$$

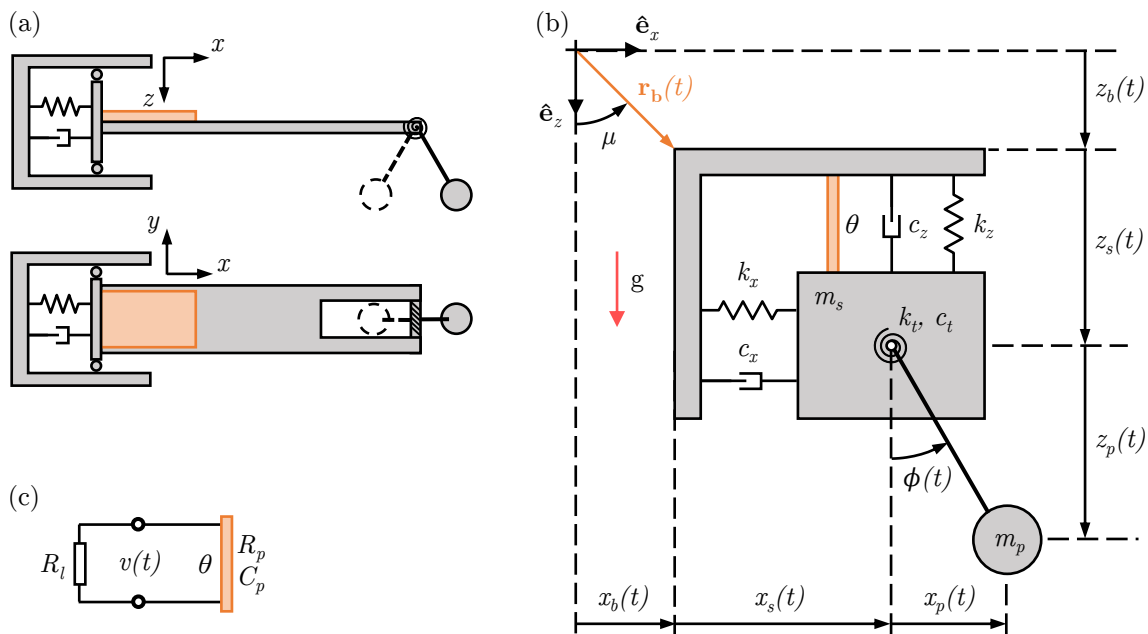


Figure 1: (a) Theoretical representation of the Oscillator-Pendulum Energy Harvester. (b) Phenomenological Model of the system. (c) Electric Circuit Representation.

The elastic and piezoelectric element behaviors are assumed to be linear and, therefore, the total restitution forces of the structure springs, the torsional spring and the piezoelectric elements attached to the structure can be defined as,

respectively:

$$f_x(t) = -k_x x(t) \quad (4)$$

$$f_z(t) = -k_z z(t) \quad (5)$$

$$f_t(t) = -k_t \phi(t) \quad (6)$$

$$f_{pzt}(t) = -k_{pzt} z(t) \quad (7)$$

The flux linkage formulation is used to find the electromechanical equations, and the relation between the flux linkage and the voltage of the system can be written as (Preumont, 2006):

$$\dot{\lambda}(t) = v(t) \quad (8)$$

in which $\lambda(t)$ and $v(t)$ are the flux linkage and the voltage, respectively.

With all the information presented so far, it is possible to calculate the energies portions of the system. The total kinetic energy can be written as the composition of the structure's and pendulum kinetic energies:

$$\begin{aligned} T = T_s + T_p &= \frac{1}{2} m_s \dot{\mathbf{r}}_s(t) \cdot \dot{\mathbf{r}}_s(t) + \frac{1}{2} m_p \dot{\mathbf{r}}_p(t) \cdot \dot{\mathbf{r}}_p(t) \\ &= \frac{1}{2} m_p \left\{ \left[\dot{x}(t) + \dot{x}_b(t) + L\dot{\phi}(t) \cos(\phi(t)) \right]^2 + \left[\dot{z}(t) + \dot{z}_b(t) - L\dot{\phi}(t) \sin(\phi(t)) \right]^2 \right\} \\ &\quad + \frac{1}{2} m_s \left\{ \left[\dot{x}(t) + \dot{x}_b(t) \right]^2 + \left[\dot{z}(t) + \dot{z}_b(t) \right]^2 \right\} \end{aligned} \quad (9)$$

The total potential energy is written as the sum of the structure and pendulum potential energies:

$$\begin{aligned} U = U_s + U_p &= - \int_0^{x_s(t)} f_x(t) dx - \int_0^{z_s(t)} f_z(t) dz - \int_0^{r_{sz}(t)} m_s g dz - \int_0^{\phi(t)} f_t(t) d\phi - \int_0^{r_{pz}(t)} m_p g dz \\ &= \frac{1}{2} k_x x(t)^2 + \frac{1}{2} k_z [z(t) + z_{st}]^2 - m_s g [z(t) + z_{st} + z_b(t)] + \frac{1}{2} k_t \phi(t)^2 \\ &\quad - m_p g [z(t) + z_{st} + z_b(t) + L \cos(\phi(t))] \end{aligned} \quad (10)$$

The dissipation of the system comes from 3 major sources: Internal viscous damping, external viscous damping and electric resistance. The first two sources can be modelled through the Rayleigh's dissipation function (D_s) in which the damping is proportional to the velocity of the system (Meirovitch, 2010). On the other hand, the dissipation function due to the equivalent electrical resistance (D_R) is written as the electrical resistance inversely proportional to the voltage:

$$D = D_s + D_R = \frac{1}{2} \left[c_x \dot{x}(t)^2 + c_z \dot{z}(t)^2 + c_t \dot{\phi}(t)^2 \right] + \frac{1}{2} \frac{\dot{\lambda}(t)^2}{R} \quad (11)$$

The total coenergy of the piezoelectric module W_e can be represented by the sum of the electrical coenergy in the capacitance W_C and the piezoelectric coenergy W_p , subtracted by the potential energy related to the restitution forces of the piezoelectric elements, U_{pzt} (Preumont, 2006):

$$W_e = W_C + W_p - U_{pzt} = \frac{1}{2} C_p \dot{\lambda}(t)^2 + \theta \dot{\lambda}(t) z(t) - \int_0^{z_s(t)} f_{pzt} dz \quad (12)$$

The Lagrangian is, then, defined as:

$$\mathcal{L} = T - U + W_e \quad (13)$$

and with the application of the method of Euler-Lagrange for 4 state variables of the system, in which 3 are mechanical and 1 is electrical:

$$\frac{d}{dt} \left(\frac{\partial \mathcal{L}}{\partial \dot{q}} \right) - \frac{\partial \mathcal{L}}{\partial q} + \frac{\partial D}{\partial \dot{q}} = 0, \quad [q = x(t), z(t), \phi(t), \lambda(t)] \quad (14)$$

Suppressing the (t) in the notation of the generalized coordinates, the Euler-Lagrange electromechanical equations of the system can be written as a system of equations dependent of x , z , ϕ and v :

$$(m_s + m_p) \ddot{x} + c_x \dot{x} + k_x x + m_p L \left[\ddot{\phi} \cos(\phi) - \dot{\phi}^2 \sin(\phi) \right] = -(m_s + m_p) \ddot{x}_b \quad (15)$$

$$(m_s + m_p) \ddot{z} + c_z \dot{z} + (k_z + k_{pzt}) z - \theta v - m_p L \left[\ddot{\phi} \sin(\phi) + \dot{\phi}^2 \cos(\phi) \right] = -(m_s + m_p) \ddot{z}_b \quad (16)$$

$$m_p L^2 \ddot{\phi} + c_t \dot{\phi} + k_t \phi + m_p L \left[\ddot{x} \cos(\phi) + (g - \ddot{z}) \sin(\phi) \right] = m_p L \left[\ddot{z}_b \sin(\phi) - \ddot{x}_b \cos(\phi) \right] \quad (17)$$

$$\theta \dot{z} + C_p \dot{v} + \frac{v}{R} = 0 \quad (18)$$

If the external forcing parameter is considered harmonic, then:

$$\mathbf{r}_b = x_b \cdot \hat{\mathbf{e}}_x + z_b \cdot \hat{\mathbf{e}}_z = A \sin(\omega t) [\sin(\mu) \cdot \hat{\mathbf{e}}_x + \cos(\mu) \cdot \hat{\mathbf{e}}_z] \quad (19)$$

Thus,

$$\ddot{\mathbf{r}}_b = \ddot{x}_b \cdot \hat{\mathbf{e}}_x + \ddot{z}_b \cdot \hat{\mathbf{e}}_z = -A\omega^2 \sin(\omega t) [\sin(\mu) \cdot \hat{\mathbf{e}}_x + \cos(\mu) \cdot \hat{\mathbf{e}}_z] \quad (20)$$

2.1 Dimensionless Electromechanical Equations

In order to generalize the analysis of the system, a normalization of units is performed. For that, a reference angle Φ , a reference voltage V , and reference frequencies of a infinitesimal oscillation around the stable equilibrium position of the system of $\omega_x = \sqrt{k_x/m_s}$, $\omega_z = \sqrt{(k_z + k_{pztz})/m_s}$, $\omega_\phi = \sqrt{g/L}$, and $\omega_t = \sqrt{k_t/(m_p L^2)}$. Considering, also, the dimensionless time $\tau = \omega_z t$ it is possible to write the dimensional coordinates in the dimensionless form as:

$$\bar{x}(\tau) = \frac{x(t)}{L}, \quad \bar{z}(\tau) = \frac{z(t)}{L}, \quad \bar{\phi}(\tau) = \frac{\phi(t)}{\Phi}, \quad \bar{v}(\tau) = \frac{v(t)}{V} \quad (21)$$

Using the chain rule, the derivatives of the dimensionless coordinates are found:

$$\dot{\bar{q}}(\tau) = \frac{d\bar{q}(\tau)}{d\tau} = \frac{d\bar{q}(\tau)}{dt} \frac{dt}{d\tau} = \frac{\dot{q}(t)}{\omega_s Q} \quad (22)$$

$$\ddot{\bar{q}}(\tau) = \frac{d\dot{\bar{q}}(\tau)}{d\tau} = \frac{d\dot{\bar{q}}(\tau)}{dt} \frac{dt}{d\tau} = \frac{\ddot{q}(t)}{\omega_s^2 Q} \quad (23)$$

in which $q = (x, z, \phi, v)$ and $Q = (L, \Phi, V)$ are dummy symbols representing the generalized coordinates and the reference measurements, respectively. Substituting the above relations in the Electromechanical Equations (15) - (18), applying some algebraic manipulations, a harmonic excitation of the form $\bar{\mathbf{r}}_b = \gamma \sin(\Omega\tau) [\sin(\Phi\bar{\mu}) \cdot \hat{\mathbf{e}}_x + \cos(\Phi\bar{\mu}) \cdot \hat{\mathbf{e}}_z]$, and considering $\Phi = 1$, the dimensionless system of electromechanical equations is found:

$$(1 + \rho) \ddot{\bar{x}} + 2\zeta_x \dot{\bar{x}} + \Omega_s^2 \bar{x} + \rho \ddot{\bar{\phi}} \cos(\bar{\phi}) - \rho \dot{\bar{\phi}}^2 \sin(\bar{\phi}) = -(1 + \rho) \ddot{\bar{x}}_b \quad (24)$$

$$(1 + \rho) \ddot{\bar{z}} + 2\zeta_z \dot{\bar{z}} + \bar{z} - \chi \bar{v} - \rho \ddot{\bar{\phi}} \sin(\bar{\phi}) - \rho \dot{\bar{\phi}}^2 \cos(\bar{\phi}) = -(1 + \rho) \ddot{\bar{z}}_b \quad (25)$$

$$\ddot{\bar{\phi}} + 2\zeta_t \dot{\bar{\phi}} + \Omega_t^2 \bar{\phi} + \Omega_\phi^2 \sin(\bar{\phi}) + \ddot{\bar{x}} \cos(\bar{\phi}) - \ddot{\bar{z}} \sin(\bar{\phi}) = \ddot{\bar{z}}_b \sin(\bar{\phi}) - \ddot{\bar{x}}_b \cos(\bar{\phi}) \quad (26)$$

$$\kappa \dot{\bar{z}} + \bar{v} + \varphi \bar{v} = 0 \quad (27)$$

in which the following dimensionless parameters arise:

$$\rho = \frac{m_p}{m_s}, \quad \zeta_x = \frac{c_x}{2\omega_z m_s}, \quad \zeta_z = \frac{c_z}{2\omega_z m_s}, \quad \zeta_t = \frac{c_t}{2\omega_z m_p L^2}, \quad \chi = \frac{\theta V}{\omega_z^2 m_s L} \quad (28)$$

$$\gamma = \frac{A}{L}, \quad \Omega = \frac{\omega}{\omega_z}, \quad \Omega_\phi = \frac{\omega_\phi}{\omega_z}, \quad \Omega_s = \frac{\omega_x}{\omega_z}, \quad \Omega_t = \frac{\omega_t}{\omega_z}, \quad \varphi = \frac{1}{\omega_z R C_p}, \quad \kappa = \frac{\theta L}{C_p V}$$

ζ_i ($i = x, z, t$) being the dissipation coefficients, related to the structure in both directions, and the torsional spring respectively. χ and κ are the piezoelectric coupling coefficients related to the mechanical and the electrical equations, respectively. Ω_k ($k = \phi, s, t$) are the reference frequency ratios in relation to the structure natural frequency in z direction. Ω is the ratio between the forcing frequency and the structure natural frequency in z direction. ρ and γ are the mass ratio and the dimensionless forcing amplitude. Finally φ is the electrical dissipation ratio of the system.

2.2 Performance Metrics

The performance of the piezoelectric energy harvesting system is evaluated with the definition of the converted electrical power by the piezoelectric element that needs to be addressed properly. Since the power is defined by the time rate of the work, the electrical output power can be defined as:

$$P_{\text{out}}^{(\text{total})} = \int_{t_0}^{t_f} \frac{v^2}{R} dt \quad (29)$$

Considering the limit of $dt = t_f - t_0 \rightarrow 0$, the instantaneous output powers is given by:

$$P_{\text{out}} = \lim_{dt \rightarrow 0} P_{\text{out}}^{(\text{total})} = \frac{v^2}{R} \quad (30)$$

The Root Mean Square (RMS) metric is adopted as the main measurement, being defined as:

$$P_{\text{out}}^{\text{RMS}} = \sqrt{\frac{1}{t_f - t_0} \int_{t_0}^{t_f} P_{\text{out}}^2 dt} \quad (31)$$

The dimensionless counterparts of equations 29, 30 and 31 are given by:

$$\bar{P}_{\text{out}}^{(\text{total})} = \int_{\tau_0}^{\tau_f} \frac{\chi\varphi}{\kappa} \bar{v}^2 \quad (32)$$

$$\bar{P}_{\text{out}} = \lim_{d\tau \rightarrow 0} \bar{P}_{\text{out}}^{(\text{total})} = \frac{\chi\varphi}{\kappa} \bar{v}^2 \quad (33)$$

$$\bar{P}_{\text{out}}^{\text{RMS}} = \sqrt{\frac{1}{\tau_f - \tau_0} \int_{\tau_0}^{\tau_f} \bar{P}_{\text{out}}^2 d\tau} \quad (34)$$

3. NUMERICAL SIMULATIONS

In this section, numerical simulations are performed employing the fourth order Runge-Kutta method to solve the nonlinear electromechanical equations. Poincaré maps and Lyapunov exponents utilizing the method proposed by (Wolf *et al.*, 1985) are employed to evaluate the dynamical characteristics of the system.

3.1 Motion Transmission

By considering the structure in its equilibrium position $(\bar{x}, \bar{z}) = (0, 0)$, and the pendulum being released from an arbitrary initial position of $\bar{\phi}$, Figure 2 shows the transmission of motion: The green curve represents the pendulum dynamics alone, while orange and red curves represents the reaction of the structure to the perturbation in the system. Blue curve represents the voltage \bar{v} generated by the motion in \bar{z} direction.

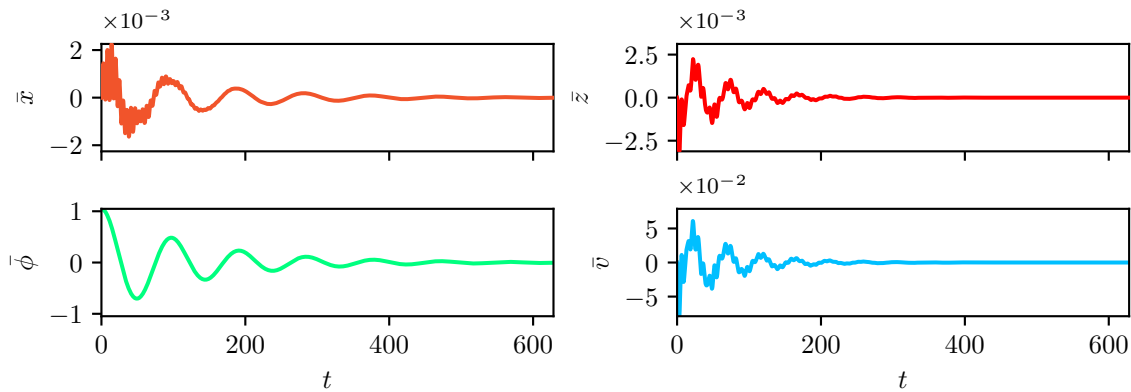


Figure 2: Dynamics of the system as the pendulum is released from an arbitrary initial position.

Now consider a scenario in which the structure is perturbed with an arbitrary initial position in \bar{x} direction, while the pendulum and the position of the structure in \bar{z} direction are at rest. Note that part of the energy entered into the system by the perturbation in the \bar{x} direction is transferred to the \bar{z} direction by the pendulum, and a part of this transferred energy is converted into electrical energy.

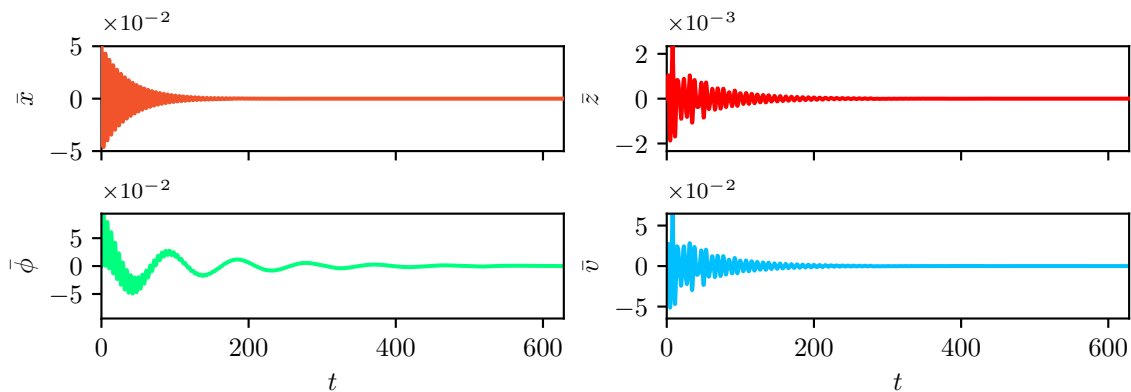


Figure 3: Dynamics of the system as the mass is released from an arbitrary x initial position.

Finally, consider a scenario in which the structure is perturbed in the \bar{z} direction, while the pendulum and the \bar{x} direction of the structure are stationary at rest. In this situation, note that neither the pendulum nor the structure in \bar{x} direction present motion, since it is an ideal system. Therefore the pendulum motion is merely dependent on the \bar{x} motion and the initial conditions, and the pendulum works as a positive passive energy absorber in \bar{x} , the direction that aggregates the energy harvesting process, making a bridge for the energy in the \bar{x} direction to reach the electrical circuit.

and the pendulum works as a energy bridge between \bar{x} and \bar{z} : The energy is absorbed from the x direction and is transferred to z direction, which, in turn, is transferred to the electric circuit, generating electrical energy. The

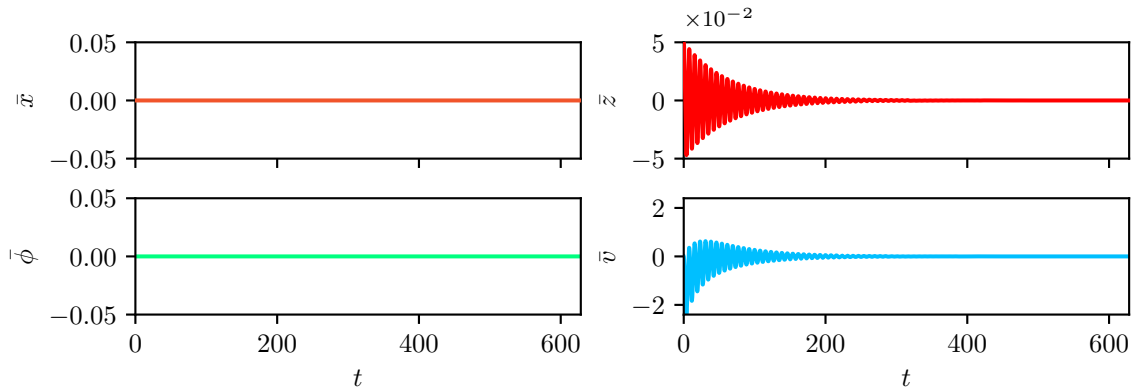


Figure 4: Dynamics of the system as the mass is released from an arbitrary \bar{z} initial position.

3.2 Bifurcation and Output Power Analysis

This section deals with the analysis of bifurcation and output power diagrams that summarize the dynamical aspects of the system in a range of frequencies. The goal is to analyze the nonlinear dynamics of the system by means of proper tools as Poincaré Maps and Lyapunov Exponents to determine the type of motion (i.e. the type of dynamical attractor). Also, the RMS output power is evaluated to determine if the changes promoted to the system by the addition of the pendulum are beneficial. Parameters utilized in the simulations are summarized in Table 1. The initial conditions of the system are redefined to its original value in each step of the simulation.

Table 1: Numerical Parameters.

Parameter	Value	Unit	Initial Condition	Value	Unit
m_s	0.005	kg	\bar{x}	0	—
m_p	0.0025	kg	$\dot{\bar{x}}$	0	—
L	0.05	m	\bar{z}	0	—
c_x	0.05	N s m ⁻¹	$\dot{\bar{z}}$	0	—
c_z	0.05	N s m ⁻¹	$\bar{\phi}$	0	—
c_t	0.00002	N s m rad ⁻¹	$\dot{\bar{\phi}}$	0	—
Ω_s	0.1 → 2.0	—	\bar{v}	0	—
Ω_ϕ	0.0678648	—			
Ω_t	0	—			
g	9.81	m/s ²			
θ	-3.985×10^{-5}	N/V			
C_p	7.2×10^{-8}	F			
R	1.1×10^6	Ω			
			Forcing Parameter	Value	Unit
			γ	0.5	—
			Ω	0 → 1.6	—
			$\bar{\mu}$	$45\pi/180$	—

Plots of the bifurcation diagrams allied with plots of the largest Lyapunov exponent (λ_1) and the classification of the type of motion of the system are a key point to understand the nonlinear dynamics of the system. Colors without legend represents the type of motion (i.e. dynamical attractor), and it is summarized in the Table 2. The methodology to classify those attractos was based on the comparison of Poincaré Map values and the sign of the two of seven (λ_1 and λ_2) largest Lyapunov exponents of the system in each iteration. If λ_1 is negative, then the Poincaré map is analyzed to determine how many forcing cycles a value repeats itself. The number of cycles determine the peridodicity of the dynamical response and if the number cycles surpass 5, the response is classified as Period-6 or greater. Nonetheless, if the λ_1 is positive and λ_2 is negative, then the system is classified as Chaotic, as only one direction in the phase space of the system is unstable. Finally, if λ_2 is also positive, then the system is classified as Hyperchaotic, as two or more directions in the phase space are unstable.

Table 2: Color legend for different attractors.

●	●	●	●	●	●	●	●
Period-1	Period-2	Period-3	Period-4	Period-5	Period-6+	Chaotic	Hyperchaotic

A set of cases are analyzed in the range of $\Omega_s = 0.1 \rightarrow 2.0$ and two of them, $\Omega_s = (0.5, 1.9)$, are chosen to summarize the most important findings. An external excitation angle of $\mu = 45$ degrees is employed in all simulations. Figures 5 and 6 show that the system dynamics is rich and complex, presenting different types of responses. Period-1, period-2, chaos and hyperchaos prevail in these cases. Regarding the power converted, the system with the pendulum (orange curve) is compared with its counterpart without the pendulum (gray curve). It is shown in Figure 5 that the addition of the pendulum for lower values of Ω_s tends to slightly increase the RMS output power in the regions right before the power peak (period-1 window near $\Omega = 0.75$), as highlighted in the zoomed region; and slightly reduces the power peak, indicating a trade-off between maximum power output and larger bandwidths. In contrast, adding the pendulum when Ω_s is higher tends to reduce the performance of the harvester, as displayed in Figure 6. This result suggests that an increase of Ω_s reduces the maximum RMS output power, as ω_x increases (increase of the stiffness of the x direction), reducing the effect of the motion amplifier in the x direction, and therefore, reducing the energy transfer between the pendulum and the structure in \bar{z} direction. Under this condition, the pendulum acts as an energy absorber. Besides, the addition of the pendulum decreases the equivalent natural frequency of the system, shifting the peak power slightly to the left.

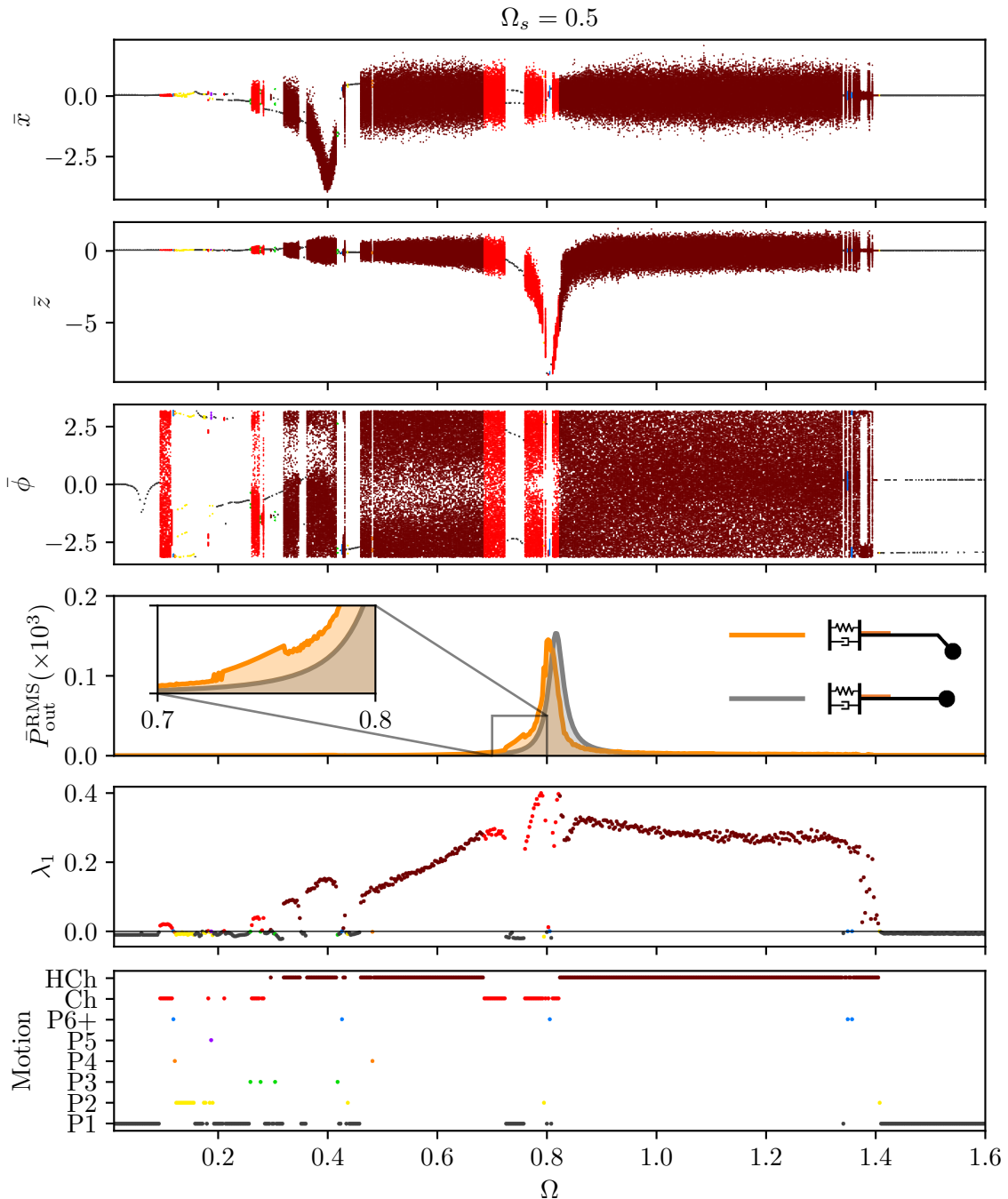


Figure 5: Bifurcation diagrams for the \bar{x} , \bar{z} and $\bar{\phi}$ directions; RMS Output Power, the largest Lyapunov exponent (λ_1) and the classification of the type of motion in a range of frequencies for $\Omega_s = 0.5$.

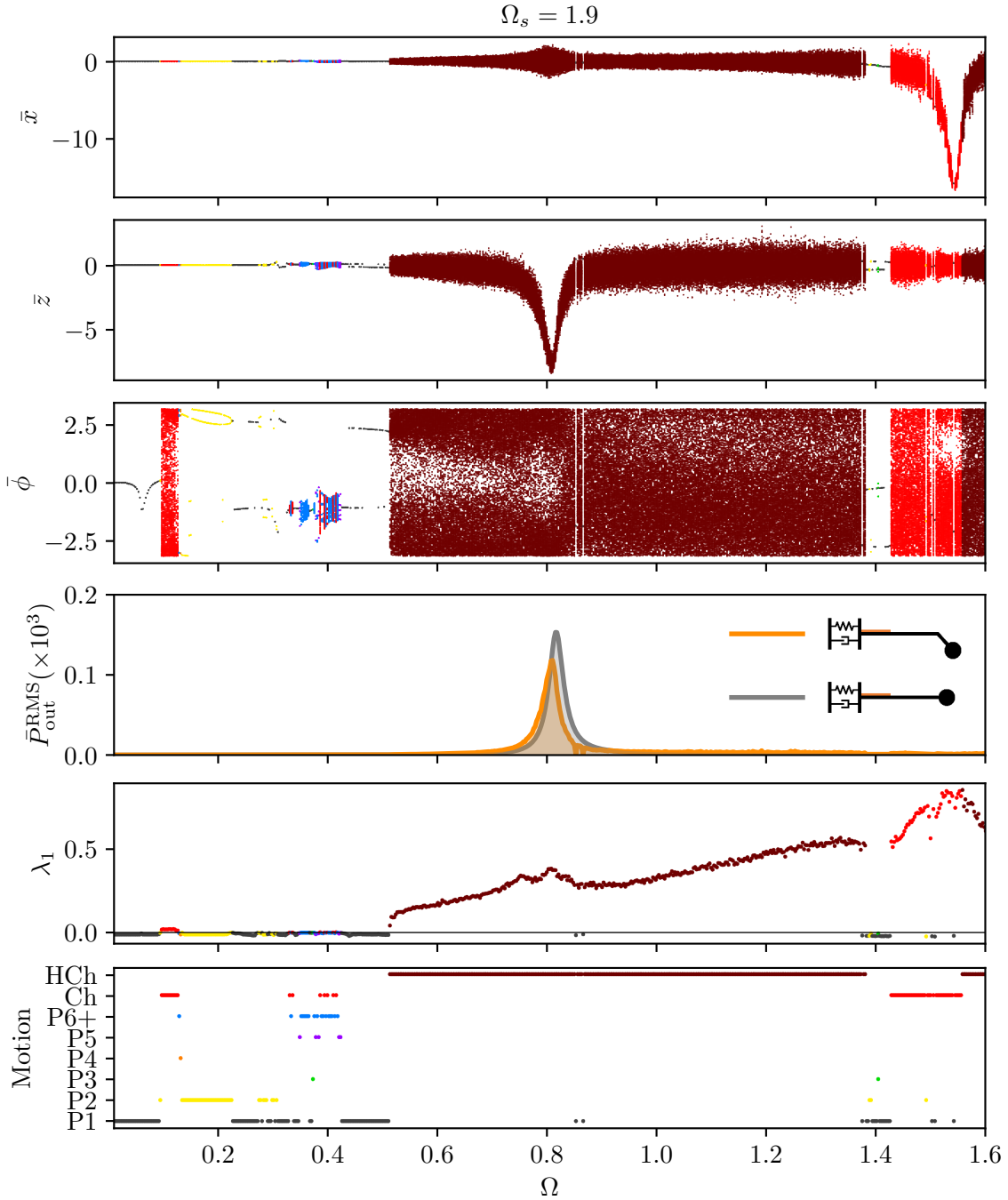


Figure 6: **Bifurcation diagrams for the x , z and ϕ directions; RMS Output Power, the largest Lyapunov exponent (λ_1) and the classification of the type of motion in a range of frequencies for $\Omega_s = 1.9$.**

To better illustrate the trade-off between the bandwidth and the maximum RMS output power, consider the area of the curve around the maximum output power as $A = \int_{\Omega_0}^{\Omega_f} \bar{P}_{\text{out}}^{\text{RMS}} d\Omega$. Figure 7 shows the difference between the areas of $\bar{P}_{\text{out}}^{\text{RMS}}$ of the proposed system (A_p) and its counterpart without the pendulum (A_{np}), as $\Delta A = A_p - A_{np}$. Note that $\Delta A \approx 0$ for $\Omega_s = 0.5$, indicating the trade-off mechanism. In contrast, for $\Omega_s = 1.9$, A_{np} is greater, indicating a decrease in the performance of the pendulum system.

It is also shown in Figure 7 a comparison between each point of the two curves. For that, a shift in the orange curve is done to match the maximum power outputs of the two cases. The blue curves show the percentage difference of the two cases, comparing the system with and without pendulum for each point in the curve. The difference metric is defined by $\text{Diff}(\%) = 100(\bar{P}_{\text{out}(p)}^{\text{RMS}} - \bar{P}_{\text{out}(np)}^{\text{RMS}})/\bar{P}_{\text{out}(np)}^{\text{RMS}}$. Positive values represent the scenarios in which the system with pendulum outperforms its counterpart, while negative values represent situations where the system without pendulum is a better choice. Note that for lower values of Ω_s , the positive values are located in regions that generates higher output powers, indicating the better performances.

Examples of phase subspaces of each one of those predominant responses are shown in Figures 8, 9, 10 and 11, in its respective colors according to Table 2. Note that there is a situation where the pendulum presents an unbounded behavior, rotating around its axis. Another interesting aspect is the difference among forms of the Poincaré map and the strange attractors of the chaotic and hyperchaotic dynamics: the chaotic strange attractor keeps a well defined

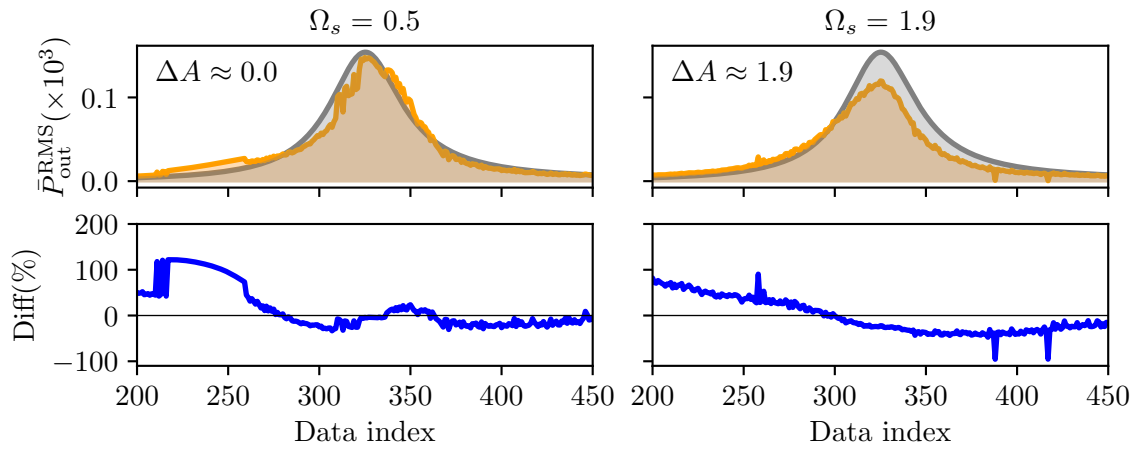


Figure 7: Comparison between the RMS output power, as the maximum values are shifted to match the same data index. Orange curves represent the system with the pendulum. Gray curves represent the system without the pendulum. The blue curves represent the difference between the orange and gray curves in each point.

fractal-like characteristic, while the hyperchaotic attractor is a shapeless cloud of points.

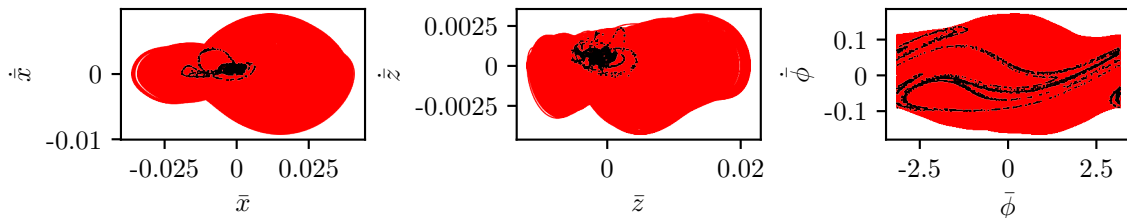


Figure 8: Phase subspaces and Poincaré maps showing a chaotic dynamics of the system for $\Omega_s = 0.7$ and $\Omega = 0.1$.

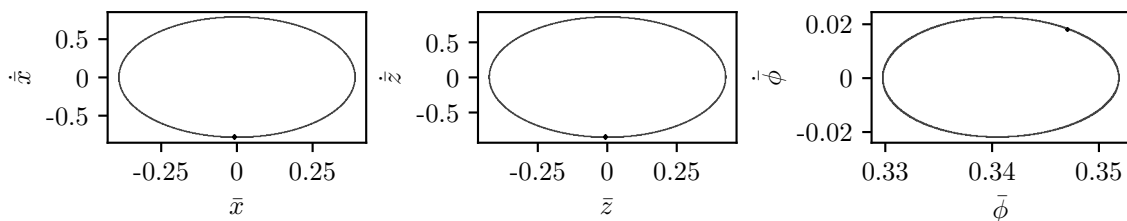


Figure 9: Phase subspaces and Poincaré maps showing a period-1 dynamics of the system for $\Omega_s = 0.7$ and $\Omega = 2$.

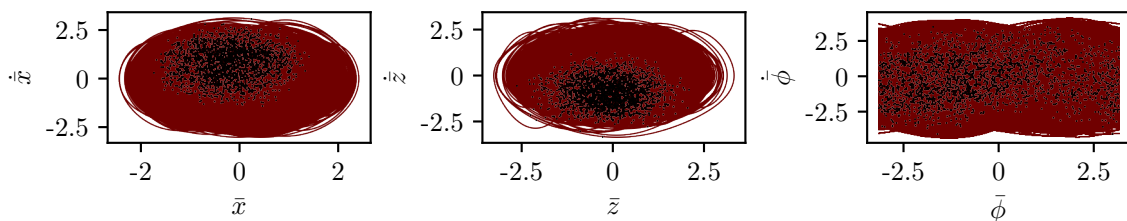


Figure 10: Phase subspaces and Poincaré maps showing a hyperchaotic dynamics of the system for $\Omega_s = 1.5$ and $\Omega = 1$.

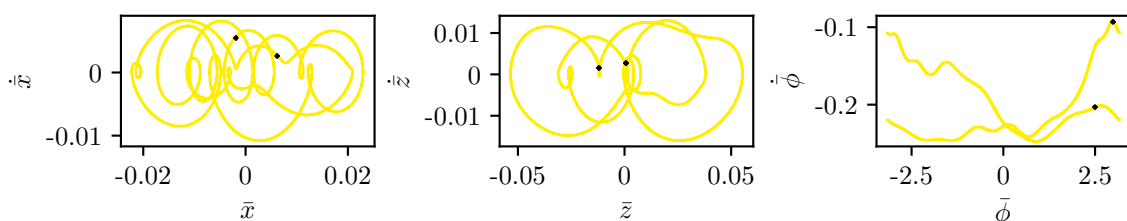


Figure 11: Phase subspaces and Poincaré maps showing a period-2 dynamics of the system for $\Omega_s = 1.5$ and $\Omega = 0.19$.

4. CONCLUSIONS

This work presents the analysis of a pendulum-oscillator energy harvester guided by a nonlinear dynamics perspective and the performance of the system. The model is based on a cantilever beam structure with an attached pendulum. The general idea of the model is to utilize the pendulum as a mean to achieve multidirectionality in the energy harvesting process. Nonlinear dynamics tools as Poincaré maps and Lyapunov exponents are employed to determine the different types of dynamical responses of the system. Results show a complex dynamics with the predominance of period-1, period-2, chaotic and hyperchaotic motions. Regarding the performance of the system, results suggest that the reduction of the frequency ratio of the structure between directions promotes a trade-off between maximum RMS output power and bandwidth, slightly increasing the bandwidth right before the natural frequency region, and slightly decreasing the maximum power output of the harvester. In contrast, the increase in the frequency ratio (that is, the increase in the stiffness in the motion amplifier) decreases the performance of the harvester, as the effects of the motion amplifier are reduced. Despite showing some potential benefits of using the pendulum to achieve multidirectionality, the increase in performance proved to be small for this set of parameters. Therefore, further investigations need to be addressed to understand the role of other key parameters in the energy harvesting process and evaluate optimized configurations.

5. ACKNOWLEDGEMENTS

The authors would like to acknowledge the support of the Brazilian Research Agencies CNPq, CAPES and FAPERJ.

6. REFERENCES

- Akin-Ponnle, A.E. and Carvalho, N.B., 2021. "Energy harvesting mechanisms in a smart city—a review". *Smart Cities*, Vol. 4, No. 2, pp. 476–498. ISSN 2624-6511. doi:10.3390/smartcities4020025.
- Costa, L.G., da Silva Monteiro, L.L., Pacheco, P.M.C.L. and Savi, M.A., 2021. "A parametric analysis of the nonlinear dynamics of bistable vibration-based piezoelectric energy harvesters". *Journal of Intelligent Material Systems and Structures*, Vol. 32, No. 7, pp. 699–723. doi:10.1177/1045389X20963188.
- Erturk, A. and Inman, D.J., 2011. *Piezoelectric Energy Harvesting*. John Wiley & Sons, Inc. ISBN 9780470682548. doi:10.1002/9781119991151.ch10.
- Kumar, K.A., Ali, S.F. and Arockiarajan, A., 2015. "Piezomagnetoelastic broadband energy harvester: Nonlinear modeling and characterization". *The European Physical Journal Special Topics*, Vol. 224, No. 14, pp. 2803–2822. doi:10.1140/epjst/e2015-02590-8.
- Liu, H., Zhong, J., Lee, C., Lee, S.W. and Lin, L., 2018. "A comprehensive review on piezoelectric energy harvesting technology: Materials, mechanisms, and applications". *Applied Physics Reviews*, Vol. 5, No. 4, p. 041306. doi:10.1063/1.5074184.
- Margielewicz, J., Gaska, D., Litak, G., Wolszczak, P. and Yurchenko, D., 2022. "Nonlinear dynamics of a new energy harvesting system with quasi-zero stiffness". *Applied Energy*, Vol. 307, p. 118159. ISSN 0306-2619. doi:https://doi.org/10.1016/j.apenergy.2021.118159.
- Meirovitch, L., 2010. *Methods of Analytical Dynamics*. Advanced engineering series. Dover Publications. ISBN 9780486432397.
- Paula, A.S.D., Inman, D.J. and Savi, M.A., 2015. "Energy harvesting in a nonlinear piezomagnetoelastic beam subjected to random excitation". *Mechanical Systems and Signal Processing*, Vol. 54-55, pp. 405 – 416. ISSN 0888-3270. doi:https://doi.org/10.1016/j.ymsp.2014.08.020.
- Pierre Curie, 1889. "Dilatation électrique du quartz". *J. Phys. Theor. Appl.*, Vol. 8, No. 1, pp. 149–168. doi:10.1051/jphysap:018890080014900.
- Preumont, A., 2006. *Mechatronics: Dynamics of Electromechanical and Piezoelectric Systems*. Springer Netherlands, Dordrecht. ISBN 978-1-4020-4696-4. doi:10.1007/1-4020-4696-0.
- Sezer, N. and Koç, M., 2021. "A comprehensive review on the state-of-the-art of piezoelectric energy harvesting". *Nano Energy*, Vol. 80, p. 105567. ISSN 2211-2855. doi:https://doi.org/10.1016/j.nanoen.2020.105567.
- Tang, X., Wang, X., Cattley, R., Gu, F. and Ball, A.D., 2018. "Energy harvesting technologies for achieving self-powered wireless sensor networks in machine condition monitoring: A review". *Sensors*, Vol. 18, No. 12. ISSN 1424-8220. doi:10.3390/s18124113.
- Wolf, A., Swift, J.B., Swinney, H.L. and Vastano, J.A., 1985. "Determining Lyapunov exponents from a time series". *Physica D: Nonlinear Phenomena*, Vol. 16, No. 3, pp. 285 – 317. ISSN 0167-2789. doi:https://doi.org/10.1016/0167-2789(85)90011-9.
- Wu, Y., Qiu, J., Zhou, S., Ji, H., Chen, Y. and Li, S., 2018. "A piezoelectric spring pendulum oscillator used for multi-directional and ultra-low frequency vibration energy harvesting". *Applied Energy*, Vol. 231, pp. 600–614. ISSN 0306-2619. doi:https://doi.org/10.1016/j.apenergy.2018.09.082.
- Zhou, Z., Qin, W. and Zhu, P., 2017. "A broadband quad-stable energy harvester and its advantages over bi-stable harvester: Simulation and experiment verification". *Mechanical Systems and Signal Processing*, Vol. 84, pp. 158 – 168. ISSN 0888-3270. doi:https://doi.org/10.1016/j.ymsp.2016.07.001.

7. RESPONSIBILITY NOTICE

The authors are solely responsible for the printed material included in this paper.